ChemComm

COMMUNICATION

View Article Online
View Journal

Cite this: DOI: 10.1039/d5cc02585k

Received 7th May 2025,
Accepted 24th June 2025

DOI: 10.1039/d5cc02585k

rsc.li/chemcomm

Air-processed efficient and pure green perovskite LEDs based on a PVP-modified NiO_x interface layer†

Jingyi Ding,[ab] Shuai Yang,[ac] Yiman Zhang,[a] Yangming Hu,[a] Wenjun Zhang,[a] Jibo Tang,[a] Hailong Wang,*[a] Qingqian Wang,*[a] Xiaobo He*[a] and Hongxing Xu[ac]

Perovskite light-emitting diodes (PeLEDs) suffer from moisture instability, which hinders their commercialization. In this study, by employing PVP-modified NiO_x films, perovskite films with improved quality and reduced trap density were obtained. The champion device achieved an EQE of 16.05%, marking the highest performance of air-processed devices reported to date.

Metal halide perovskites (MHPs) are potential semiconductor materials for light-emitting diode applications. The exceptional opto-electronic properties of MHPs, such as tunable bandgaps, near-unity photoluminescence quantum yields (PLQYs), and narrow emission peaks, enable perovskite light-emitting diodes (PeLEDs) to be promising for novel lighting and display devices.[1–10] The state-of-the-art green and red PeLEDs have achieved external quantum efficiencies (EQEs) exceeding 30% and the EQE of blue PeLEDs has also surpassed 20%.[11–13] Despite the great improvement of PeLED device performance, the deposition process of high-quality perovskite films still relies on an inert gas atmosphere. The moisture sensitivity of MHPs increases the device fabrication complexity and cost, which hinders their industrial manufacturing. Thus, the deposition of high-quality MHP thin films in an ambient atmosphere would be significant for PeLED applications.

To achieve this goal, different strategies have been employed in recent years. Liu *et al.* restrained phase aggregation in MHP thin films through antisolvent engineering.[14] Compact morphology and homogeneous phase distribution were obtained by adding diethyl ether (DEE) as an antisolvent, which led to a green PeLED device with an EQE of 15.4%. Li *et al.* applied different self-assembled monolayers (SAMs) as hole transport layers (HTLs), replacing the most commonly used PEDOT:PSS.[15] The modified thin film exhibited improved morphology and the EQE and brightness of the devices were increased. Based on this, the same group improved the device performance of green PeLEDs and achieved blue PeLEDs through interfacial engineering.[16–18] However, the emission peak wavelength of the reported air-processed green PeLEDs is no larger than 525 nm, which does not comply well with the Rec. 2020 standard for display applications.

In this work, we fabricated efficient and pure green PeLEDs by employing a structure that incorporates $FAPbBr_3$ emissive layers coated on a polyvinyl pyrrolidone (PVP)-modified NiO_x substrate, processed under ambient air conditions. Incorporating PVP between the NiO_x and perovskite layers enhanced the film crystallization quality of the perovskite. This enhancement was attributed to the improved filtration of the perovskite precursor solution on the substrate, leading to a more uniform morphology and larger grain sizes within the perovskite layer. Furthermore, introducing PVP reduced the trap density, effectively inhibiting non-radiative recombination processes. As a result, the photoluminescence (PL) properties of the perovskite emissive layers were markedly enhanced. The resultant PeLEDs exhibited a pure green emission peak at 535 nm, with CIE coordinates of (0.22, 0.75) and a full width at half-maximum (FWHM) of 21 nm. The operational stability of the devices was improved. Notably, the champion device achieved an EQE of 16.05%, which represents a new record among all reported air-processed green PeLEDs.

Fig. 1a shows the typical spin-coating method of HTL and perovskite thin films. EA in TPPO was used as an anti-solvent for perovskite thin film deposition. HTLs, the PVP interlayer and perovskite emitters were all spin-coated in the air with 50 ± 5% humidity. Deionized water was spin-coated to reduce the thickness of NiO_x, aiming to inhibit PL quenching at the

[a] *Institute of Physics, Henan Academy of Sciences, Zhengzhou, China. E-mail: wanghailong@hnas.ac.cn, wangqingqian@hnas.ac.cn, hexiaobo@hnas.ac.cn*

[b] *College of Electronic and Electrical Engineering, Henan Normal University, Zhengzhou, China*

[c] *School of Future Technology, Henan University, Zhengzhou, China*

† Electronic supplementary information (ESI) available: Experimental methods, transmittance spectra, PL spectra, XPS and UPS spectra, SEM and AFM images of NiO_x, current efficiency, stability, statistics and performance summary table of devices. See DOI: https://doi.org/10.1039/d5cc02585k

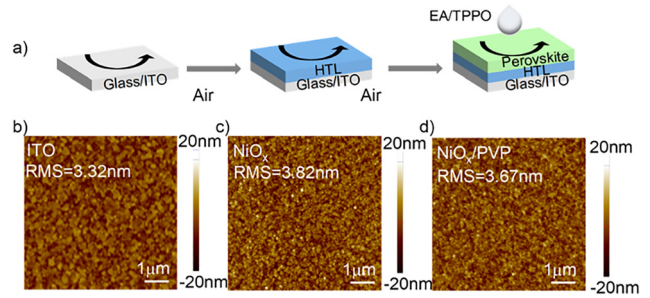

Fig. 1 (a) Schematic of perovskite thin film preparation in an air environment. (b)–(d) AFM images of ITO, NiO_x and NiO_x/PVP.

interface[19,20] (Fig. S1, ESI†). The results of AFM, XPS, and transmittance spectroscopy reveal the effect of deionized water treatment and PVP modification on NiO_x (Fig. 1b–d and Fig. S2, S3, ESI†). The AFM images of ITO, NiO_x, and NiO_x/PVP are shown in Fig. 1b–d. The root mean square (RMS) roughness values of NiO_x and NiO_x/PVP are 3.82 nm and 3.67 nm, respectively, which are not significantly different from that of ITO glass (3.32 nm). These differences in RMS roughness among NiO_x, NiO_x/PVP, and ITO glass indicate the successful deposition of NiO_x and PVP layers. XPS tests were also performed to verify that the NiO_x was not rinsed out after treatment with deionized water and PVP solutions. As shown in Fig. S2 (ESI†), the peaks of Ni imply the existence of NiO_x and it is reasonable that the N peak appears only on NiO_x/PVP. The transmittance spectra (Fig. S3, ESI†) of NiO_x and NiO_x/PVP exhibit curves with little difference, indicating high and equal light extraction efficiency.

PVP modification significantly affects the NiO_x/perovskite interface. The contact angle of the perovskite precursor on the NiO_x/PVP substrate (19.7°) is almost half that of the precursor on the NiO_x substrate (36.7°), as shown in Fig. 2a. As a result, the perovskite thin film deposited on NiO_x/PVP displays better morphology with a more uniform and denser surface (Fig. 2b and c) than on NiO_x. The XRD patterns (Fig. 2d) exhibit a much higher peak intensity of the perovskite on NiO_x/PVP, indicating higher crystallinity of the perovskite on NiO_x/PVP. The two peaks at 2θ of 14.499° and 29.643° belong to the (100) and (200) facets of $FAPbBr_3$, respectively. The FWHM values of the NiO_x/PVP sample are 0.47° and 0.56°, which are smaller than those of the NiO_x sample (both values are 0.60°). According to the Scherrer formula,[21] we can know, $D \propto 1/\beta$, where D is the crystal size and β is the FWHM. Thus, the decreased FWHM values indicate that the crystal size of the NiO_x/PVP sample is larger than that of the NiO_x sample (Fig. S5, ESI†). Meanwhile, the smaller FWHMs and larger grain sizes also verify the higher crystallinity of the perovskite on NiO_x/PVP. The absorption and steady state PL spectra of NiO_x and NiO_x/PVP samples are shown in Fig. 2e and f. Both the absorption and PL peaks of the NiO_x/PVP sample exhibit a red shift of 10 nm compared to the NiO_x sample, which can be attributed to the larger crystal size in the NiO_x/PVP sample. UPS results reveal the energy landscape of NiO_x with and without PVP modification (Fig. S4, ESI†), NiO_x (−5.32 eV) and PVP-modified NiO_x (−5.38 eV).

The TRPL measurements were carried out to investigate the carrier dynamics in the perovskite on different interfaces. The PL decays are shown in Fig. 3a. Obviously, the NiO_x/PVP sample exhibits a much longer PL lifetime compared to the NiO_x sample. The τ_{avg} on NiO_x/PVP is 59.22 ns, which is one order of magnitude higher than that on NiO_x (4.85 ns). Details of decay fitting are shown in Table S1 (ESI†). The improved PL lifetime is attributed to the higher crystallinity and quality of thin films, indicating reduced trap density. Meanwhile, the PLQY also increases from 28.8% to 49.3% (Fig. 3b). XPS results of the two samples confirm the interaction between PVP and the perovskite (Fig. S7, ESI†). The characteristic peaks at around 141 eV and 138 eV belong to Pb $4f_{7/2}$ and $4f_{5/2}$ of Pb–Br in perovskite films (Fig. S7f, ESI†). This little shift is ascribed to the change in the electron cloud density,

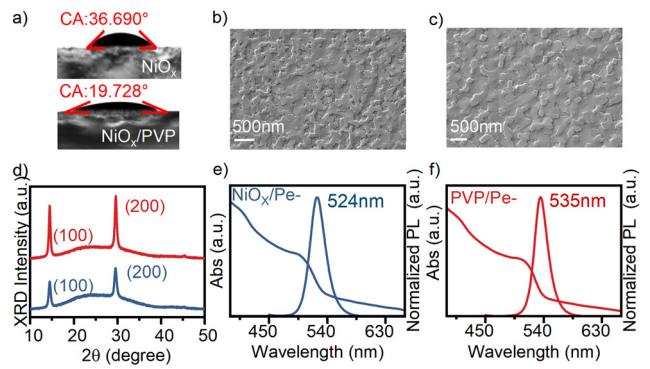

Fig. 2 Optical micrographs of perovskite precursor solutions on NiO_x substrates without/with PVP modification (a). SEM images of perovskite layers deposited on (b) NiO_x and (c) NiO_x/PVP substrates. (d) XRD patterns of perovskite layers deposited on NiO_x and NiO_x/PVP substrates. (e) and (f) UV absorption and PL spectra of perovskite thin films deposited on NiO_x and NiO_x/PVP substrates.

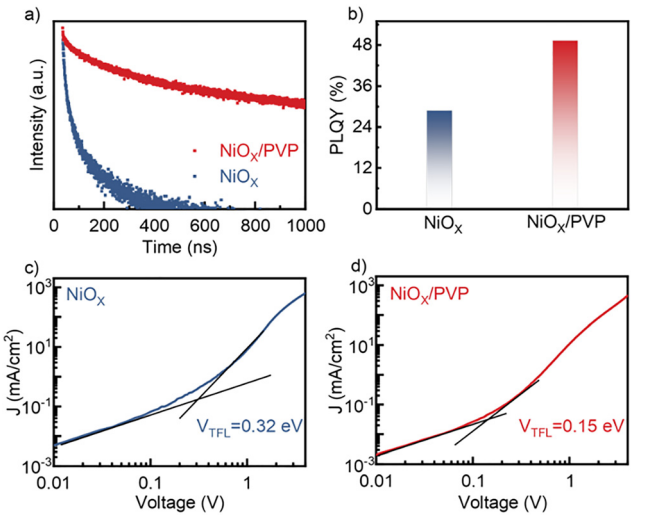

Fig. 3 TRPL and PLQY results of perovskite layers deposited on pristine (a) and PVP-modified (b) NiO_x substrates. (c) and (d) J–V curves of hole-only devices with the device structure of ITO/NiO_x or PVP-modified NiO_x/perovskite/MoO_x/Au.

indicating the interaction between PVP and the perovskite.[22–24] The valence band energy of the perovskite films is shown in Fig. S8 (ESI†), which is −5.56 eV and −5.53 eV for perovskite/NiO_x and perovskite/PVP-NiO_x, respectively. To further understand the trap state change in perovskite films, we fabricate and characterize hole-only devices with a structure of ITO/NiO_x or PVP-modified NiO_x/perovskite/MoO_x/Au. The trap-filled limit point in the *J–V* curves of the hole-only device marks the transition from trap-dominated to free-carrier-dominated conduction. From the *J–V* curves of the two samples, we can see that the V_{TFL} of the pristine device is 0.32 V, which is more than twice that of the PVP-modified one (0.15 V). Since $N_t \propto V_{TFL}$, the PVP-modified device has a trap density less than half that of the pristine device, which also confirms the reduced defect density and increased crystallinity of PVP-modified perovskite thin films.

The encouraging results prompted the fabrication of PeLEDs in the air environment, utilizing a device architecture comprising ITO/NiO_x or PVP-modified NiO_x/perovskite/TPBi/LiF/Al (see Fig. 4a and the cross-sectional image in Fig. S9, ESI†). Current density and luminance as a function of voltage are plotted in Fig. 4b. The turn-on voltage at a luminance of 1 cd m^{-2} (V_T) and maximum luminance (L_{max}) are 2.9 V and 15 856 cd m^{-2} for NiO_x-based PeLEDs and 2.8 V and 12 004 cd m^{-2} for PVP-modified NiO_x-based PeLEDs (Table S2, ESI†). The superior charge carrier density and electroluminescence brightness observed in NiO_x/PVP-based devices are attributed to optimized hole injection, as confirmed by the significantly reduced valence band offset (ΔE = 0.15 eV *vs.* 0.24 eV at unmodified interfaces, exhibiting a 37.5% reduction). This interfacial engineering effectively minimizes energy barriers for hole transport.[27] Notably, devices employing PVP-modified NiO_x demonstrate significantly reduced dark current, nearly two orders of magnitude lower when the operating voltage is below 2.6 V. This reduction can be attributed to the dense surface morphology of the perovskite thin film deposited on the PVP-modified NiO_x substrate. Furthermore, benefiting from the enhanced photoluminescent properties of the perovskite thin film, the PVP-modified NiO_x-based devices achieve a maximum external quantum efficiency (EQE_{max}) of 16.05%, marking a 52% increase relative to the EQE_{max} of 10.55% observed in NiO_x-based devices (Fig. 4c and Table S2, ESI†). The EL peaks of both devices are located at 535 nm with CIE coordinates of (0.22, 0.75) and a FWHM of 21 nm, indicative of pure green light emission (Fig. 4d, e and Table S2, ESI†). As corroborated by prior reports, PVP-modified NiO_x-based devices achieve the highest EQE among air-processed green PeLEDs and comply with the Rec. 2020 standard (Fig. 4f and Table S3, ESI†). Additionally, the PVP modification substantially enhances the operational stability of the device when operated at an initial luminance of 100 cd m^{-2} (Fig. S12, ESI;† the PL stability of the perovskite films are shown in Fig. S11, ESI;† the PL intensity maintains ~70% of its initial value after 7 hours of continuous air exposure). Statistical analysis of 25 individual devices indicates that the PVP-modified NiO_x-based devices exhibit an average EQE_{max} of 14.14%, which is 2.4 times greater than the average EQE_{max} of 5.95% observed in NiO_x-based devices (Fig. S13, ESI†). This suggests that PVP-modified NiO_x serves as an HTL, facilitating improved reproducibility in the fabrication of air-processed PeLEDs.

Although we have successfully achieved high performance green PeLEDs processed under air conditions, the main parameters of the devices are still significantly inferior to recent devices fabricated under inert gas conditions.[28] The performance differences between the two kinds of PeLEDs arise from moisture-induced accelerated crystallization, which compromises the perovskite film quality. To mitigate this, we propose (1) shielding active layers from airborne moisture by employing low-hygroscopicity bottom interfacial layers and (2) modulating crystallization kinetics using strongly interacting additives. These approaches are anticipated to enhance morphological control and environmental stability in air-fabricated PeLEDs.[16,29]

In summary, we present the development of highly efficient air-processed pure green PeLEDs, achieving an EQE of 16.05%, which represents the highest performance recorded for air-processed green PeLEDs to date. This enhancement is attributable to the strategic modification of the interface between the perovskite layer and the hole transport layer (HTL) substrate using PVP. The incorporation of PVP significantly improves the crystallinity of the perovskite emissive layers, which in turn leads to a reduction in defect density. Furthermore, perovskite films deposited on PVP-modified NiO_x substrates exhibit enhanced PLQYs and extended PL lifetimes. As a result, devices based on the PVP-modified NiO_x substrate achieve a maximum EQE of 16.05%.

This work was supported by National Natural Science Foundation of China (No. 62405085) and High-level Talent Research Start-up Project Funding of Henan Academy of Sciences (No. 231720005, No. 231820060).

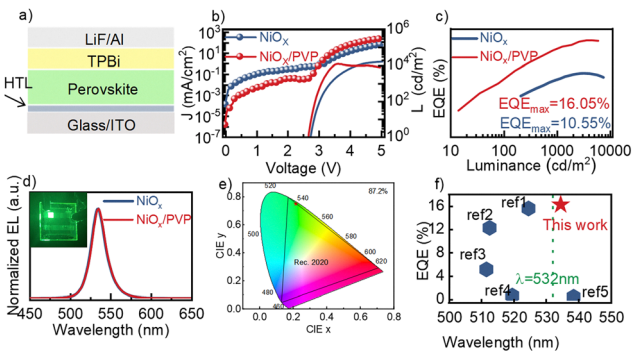

Fig. 4 Device structure of PeLEDs (a), *J–V–L* curves (b), EQE as a function of luminance (c) and EL spectra (d) of NiO_x and PVP-modified NiO_x based devices. (e) CIE coordinates of the EL from the PVP-modified NiO_x based device. (f) Summary of the state-of-the-art air processed green PeLEDs based on EQE_{max} and peak wavelength.[14–16,25,26]

Conflicts of interest

There are no conflicts to declare.

Data availability

The data supporting this article have been included as part of the ESI.†

Notes and references

1 M. Ghasemi, J. Lu, B. Jia and X. Wen, *Chem. Soc. Rev.*, 2025, **54**, 1644–1683.
2 H. Dong, C. Ran, W. Gao, M. Li, Y. Xia and W. Huang, *eLight*, 2023, **3**, 3.
3 Y. Wang, Y. Wang, T. A. S. Doherty, S. D. Stranks, F. Gao and D. Yang, *Nat. Rev. Chem.*, 2025, **9**, 261–277.
4 A. Fakharuddin, M. K. Gangishetty, M. Abdi-Jalebi, S.-H. Chin, A. R. bin Mohd Yusoff, D. N. Congreve, W. Tress, F. Deschler, M. Vasilopoulou and H. J. Bolink, *Nat. Electron.*, 2022, **5**, 203–216.
5 Y. Liu, S. Wang, Z. Yu, G. Chen, C. Wang, T. Wang, W. Ke and G. Fang, *Adv. Mater.*, 2023, **35**, 2302161.
6 J. Jiang, M. Shi, Z. Xia, Y. Cheng, Z. Chu, W. Zhang, J. Li, Z. Yin, J. You and X. Zhang, *Sci. Adv.*, 2024, **10**, eadn5683.
7 L. N. Quan, B. P. Rand, R. H. Friend, S. G. Mhaisalkar, T.-W. Lee and E. H. Sargent, *Chem. Rev.*, 2019, **119**, 7444–7477.
8 Y.-H. Kim, J. S. Kim and T.-W. Lee, *Adv. Mater.*, 2019, **31**, 1804595.
9 J. Li, P. Du, Q. Guo, L. Sun, Z. Shen, J. Zhu, C. Dong, L. Wang, X. Zhang, L. Li, C. Yang, J. Pan, Z. Liu, B. Xia, Z. Xiao, J. Du, B. Song, J. Luo and J. Tang, *Nat. Photon.*, 2023, **17**, 435–441.
10 D. Zhang, L. Chao, G. Jin, Z. Xing, W. Hong, Y. Chen, L. Wang, J. Chen and D. Ma, *Adv. Funct. Mater.*, 2022, **32**, 2205707.
11 S.-C. Feng, Y. Shen, X.-M. Hu, Z.-H. Su, K. Zhang, B.-F. Wang, L.-X. Cao, F.-M. Xie, H.-Z. Li, X. Gao, J.-X. Tang and Y.-Q. Li, *Adv. Mater.*, 2024, **36**, 2410255.
12 S.-Q. Sun, J.-W. Tai, W. He, Y.-J. Yu, Z.-Q. Feng, Q. Sun, K.-N. Tong, K. Shi, B.-C. Liu, M. Zhu, G. Wei, J. Fan, Y.-M. Xie, L.-S. Liao and M.-K. Fung, *Adv. Mater.*, 2024, **36**, 2400421.
13 Y. Gao, Q. Cai, Y. He, D. Zhang, Q. Cao, M. Zhu, Z. Ma, B. Zhao, H. He, D. Di, Z. Ye and X. Dai, *Sci. Adv.*, 2024, **10**, eado5645.
14 Y. Liu, T. Bu, L. K. Ono, G. Tong, H. Zhang and Y. Qi, *Adv. Funct. Mater.*, 2021, **31**, 2103399.
15 W. Li, T. Li, Y. Tong, H. Qi, Y. Zhang, Y. Guo, H. Wang, H. Wang, K. Wang and H. Wang, *ACS Appl. Mater. Interfaces*, 2023, **15**, 36602–36610.
16 H. Li, J. Wu, S. Hu, W. Zhang, J. Gao, Y. Guo, P. Guo, C. Liu, G. Zhao, M. Fu, H. Bian, T. Liu, H. Wang and H. Wang, *Adv. Funct. Mater.*, 2023, **33**, 2303787.
17 W. Li, T. Li, Y. Tong, Y. Li, H. Wang, H. Qi, K. Wang and H. Wang, *Adv. Funct. Mater.*, 2024, **34**, 2311133.
18 Y. Guo, H. Li, P. Yang, J. Gao, Z. Cheng, F. Dong, J. Wu, H. Wang and H. Wang, *Chem. Eng. J.*, 2024, **490**, 151764.
19 H. Wang, Y. Xu, L. Chen, J. Wu, Q. Wang, B. Zhang and Z. Xie, *Org. Electron.*, 2021, **98**, 106299.
20 H. Wang, X. Tang, G. Sun, D. Chen, Z. Ye, Y. Liu and Y. Jin, *J. Phy. Chem. Lett.*, 2023, **14**, 5827–5833.
21 A. L. Patterson, *Phys. Rev.*, 1939, **56**, 978–982.
22 Z. Wang, X. Xu, L. Gao, X. Yan, L. Li and J. Yu, *Nanoscale Res. Lett.*, 2020, **15**, 34.
23 W. Feng, Y. Zhao, K. Lin, J. Lu, Y. Liang, K. Liu, L. Xie, C. Tian, T. Lyu and Z. Wei, *Adv. Funct. Mater.*, 2022, **32**, 2203371.
24 Z. Chu, Q. Ye, Y. Zhao, F. Ma, Z. Yin, X. Zhang and J. You, *Adv. Mater.*, 2021, **33**, 2007169.
25 T. Kim, J.-H. Kim and J.-W. Park, *Phys. Status Solidi A*, 2019, **216**, 1900642.
26 P. Cheng, Z. Liu, R. Kang, J. Zhou, J. Zhao and Z. Zuo, *Phys. Status Solidi RRL*, 2023, **17**, 2200295.
27 R. Wang, X. Liu, S. Yan, N. Meng, X. Zhao, Y. Chen, H. Li, S. M. H. Qaid, S. Yang and M. Yuan, *et al.*, *Nat. Commun.*, 2024, **15**, 8899.
28 A. Yu, J. Wang, Y. Huo, S. Wang, X. Zhang, T. He, S. Yang, Y. Jiang, L. Zhang and Z. Liu, *et al.*, *Adv. Mater.*, 2025, 2503704.
29 Y. Tong, Y. Wang, H. Qi, P. Pang, Z. Sheng, Y. Liu, G. Xing, K. Wang and H. Wang, *Nano Lett.*, 2025, **25**, 8834–8842.

